Communication

Journal of Photopolymer Science and Technology
Volume 31, Number 2 (2018) 243 – 247 ©2018SPST

Photo-induced Fragmentation of a Tin-oxo Cage Compound

Jarich Haitjema[1], Lianjia Wu[1], Alexandre Giuliani[2,3], Laurent Nahon[3], Sonia Castellanos[1], and Albert M. Brouwer[1,4*]

[1]Advanced Research Center for Nanolithography, P.O. Box 93019, 1090 BA Amsterdam, the Netherlands
[2]UAR 1008 CEPIA, INRA, F-44316 Nantes, France
[3]Synchrotron SOLEIL, L'Orme des Merisiers, BP 48 Saint Aubin, 91192 Gif-sur-Yvette, France
[4]University of Amsterdam, van't Hoff Institute for Molecular Sciences, P.O. Box 94157, 1090 GD Amsterdam, the Netherlands
**f.brouwer@arcnl.nl*

Tin-oxo cage materials are of interest for use as photoresists for EUV (Extreme-Ultraviolet) lithography (13.5 nm, 92 eV), owing to their large absorption cross section for EUV light. In this work we exposed an *n*-butyl tin-oxo cage dication in the gas phase to photons in the energy range 4-14 eV to explore its fundamental photoreactivity. At all energies above the onset of electronic absorption at ~5 eV (~250 nm) cleavage of tin-carbon bonds was observed. With photon energies >12 eV (<103 nm) photoionization can occur, leading to 3+ ions. Besides the higher charge promotion, butyl chain loss without electron ejection (leading to 2+ fragments) still occurs.
Keywords: Tin-oxo cage, Photoresist, Mass spectrometry, Photochemistry

1. Introduction

Photoresists that are specifically designed for extreme ultraviolet (EUV, 13.5 nm) radiation have attracted considerable interest recently [1-3]. For instance, incorporating metal atoms in the resist formulation can increase the EUV absorption considerably [4,5]. This may lead to enhanced sensitivity and remove the need for a photo-acid generator, used to enhance the effect of the photoreaction in Chemically Amplified Resists. A photoresist without photo-acid generators may have considerably lower chemical noise, because the photo-acids (and quenchers) have an inherent random distribution within the photoresist layer, and acid diffusion contributes to blurring of the pattern [6,7]. Most importantly, strong absorption of the photoresist allows the use of thinner layers. Smaller aspect ratios can then be achieved, which are more suitable for small critical dimensions, because they are less prone to pattern collapse [8]. Therefore, a highly absorbing photoresist without photo-acid generators may have considerably better photoresist performance in terms of the well-known parameters resolution (scale of patterning), sensitivity (number of photons needed) and line edge roughness (deviation of the patterning from perfectly straight lines).

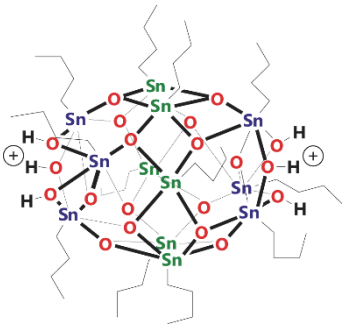

Fig. 1. Tin-oxo cage dication structure.

An example of such a material is the tin-oxo cage (see Fig. 1) [9-11]. This cage consists of a tin-oxo core with 12 organic groups (in the present case *n*-butyl chains) attached to the tin atoms. The

Received April 6, 2018
Accepted May 17, 2018

absorption of a thin film of this material at 13.5 nm is very high (~13 μm^{-1} compared to ~5 μm^{-1} for conventional resists based on organic polymers) [12]. The tin-oxo cage materials turn insoluble upon EUV radiation, thus having the properties of a negative tone resist. The solubility change upon irradiation also occurs for electron-beam and UV radiation. The mechanism behind the solubility change of the tin-oxo cages (and related materials) is still under investigation. Knowledge of the chemical mechanism is paramount for the design of novel metal-containing materials with even better resist performance [13]. Ideally, one would expose the photoresist to EUV radiation and analyze the reaction products afterwards, or even in situ. However, the analysis of chemical changes in nanometric films is challenging and a combination of surface analysis and other techniques is necessary to unequivocally identify the products of radiation.

Another way to study the reaction mechanism is through gas-phase photofragmentation experiments on trapped ionic species [14-17]. The bare cage can conveniently be isolated in the gas phase as the 2+ ion (Fig. 1) using electrospray and trapped in a linear ion trap or quadrupole trap [18]. In the present work we exposed the trap content to UV and VUV radiation and analyzed the products by means of mass spectrometry. Using this method, the fragmentation pathways in the gas phase can be elucidated. While further reaction steps occur in a photoresist film, the gas phase experiments pinpoint reactive sites within the molecule and allow us to elucidate the initial reaction steps.

2. Experimental

The tin-oxo cage $[(n\text{BuSn})_{12}O_{14}(OH)_6]^{2+}(X^-)_2$, where X^- denotes a counterion, was prepared according to previously described methods [10,11,19], starting from the commercially available *n*BuSnOOH (Sigma Aldrich) and *p*-toluene sulfonic acid (Sigma Aldrich) to yield $[(n\text{BuSn})_{12}O_{14}(OH)_6](p\text{Tos})_2$ which was then exchanged with aqueous base to yield $[(n\text{BuSn})_{12}O_{14}(OH)_6](OH)_2$ which we call TinOH. NMR and IR spectra agreed with the literature. Absorption measurements were recorded with a Shimadzu 2700 spectrometer, using spectroscopic grade ethanol (EtOH) as a solvent.

The compound TinOH was dissolved in methanol (concentration ~10 µM), filtered and electrosprayed for the gas phase VUV exposure experiments, using a syringe pump with a flow rate of about 5 µL/min. Ions with *m/z* 1218 were trapped in a commercial linear ion trap (Thermo Finnigan LTQ XL) coupled [20] to the DESIRS VUV beamline [21] of the SOLEIL synchrotron. The VUV photons were monochromatic and high harmonics-free owing to the use of a Kr gas filter and a quartz window when necessary. A mechanical shutter coupled to the mass analyzer was used to control irradiation of the trapped ions between 500 and 2000 ms. The photon flux was in the 10^{12}-10^{13} photon/sec range and was measured independently using an AXUV100 photo diode (International Radiation Detectors) under the same conditions and used to normalize the spectra. The irradiation time and photon flux were kept low enough to avoid absorption by the photoproducts.

3. Results and discussion

3.1. Mass spectrum

The mass spectrum of the tin cage was reported earlier by Dakternieks et al. [18], who also observed the main peak at *m/z* 1218. This peak is quite broad due to the 10 stable isotopes of Sn. The high mass resolution of our instrumentation allowed us to resolve the isotope pattern (see Fig. 2). This pattern reveals the 2+ charge, because the spacing between the peaks is half an *m/z* unit.

Depending on electrospray conditions, a peak with a lower *m/z* (1190) also appeared in the mass spectrum. This belongs to the tin cage where one of the butyl chains has been lost. By tuning the electrospray ion source and applying a mass filter, we made sure that only $[(n\text{BuSn})_{12}O_{14}(OH)_6]^{2+}$ was present in the ion trap as a parent species.

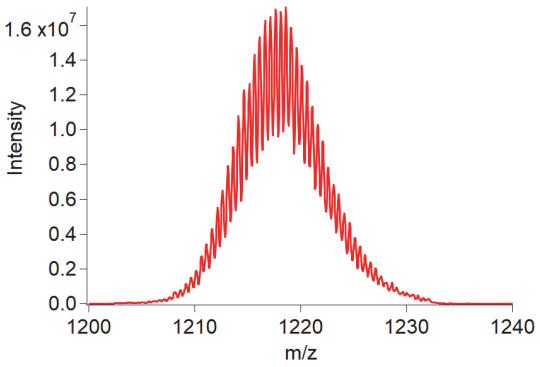

Fig. 2. Electrospray ionization (ESI) Mass spectrum of $[(n\text{BuSn})_{12}O_{14}(OH)_6]^{2+}$, showing a main peak centered at *m/z* = 1218 and a broad isotope pattern.

3.2. UV and VUV irradiation experiments

In an initial set of experiments, we exposed the tin cage to UV light ranging from 4 to 7 eV (310 nm to 177 nm). In this range the tin cage in solution shows a strong absorption centered around 220 nm [22]. The Highest Occupied Molecular Orbital (HOMO) is primarily located on the six-coordinated Sn atoms and has a Sn-C σ-bonding character. The LUMO is located on the central belt of the cage and consists mainly of Sn *d*-orbitals. The tin cage was previously shown to undergo photoreactions upon 225 nm exposure in solution, but the photoproducts could not yet be firmly identified [22]. We aim here at shedding light onto the photofragmentation in the gas phase, i.e. onto the intrinsic reactivity of the isolated ion.

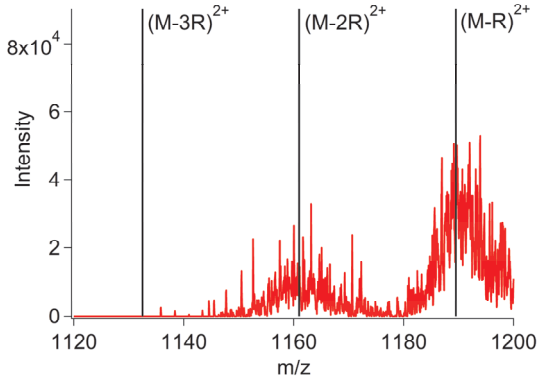

Fig. 3. Mass spectrum with 7 eV (177 nm) incident photon energy at *m/z* values just below the parent peak (*m/z* 1218). Vertical lines indicate the *m/z* corresponding to loss of butyl (R groups): M-3R (*m/z* 1132.5), M-2R (*m/z* 1161) and M-R (*m/z* 1189.5).

The fragmentation spectrum of the tin-oxo cage at 7.0 eV is shown in Fig. 3. It can be seen that the main peak (M) easily loses a butyl chain (R) upon excitation. This indicates cleavage of Sn-C bonds as the primary process in the electronically excited state. The isotope pattern shows that the fragments have a 2+ charge. It can be seen that one or two butyl chains are lost, but there are no peaks corresponding to loss of three or more butyl chains. The fragmentation yield (measured by the peak integrals, corrected for the photon flux) peaks around 225 nm and then decreases to almost zero going to lower energy (longer wavelength). There is essentially no photon absorption below ~5 eV (~250 nm). These results agree with previous measurements of spectra in solution (see Fig. 4). The overall shape of the spectrum is the same in both cases. At wavelengths <200 nm no solution absorption spectrum could be recorded, due to the cutoff wavelength of the solvent used (EtOH). The gas phase experiment, however,

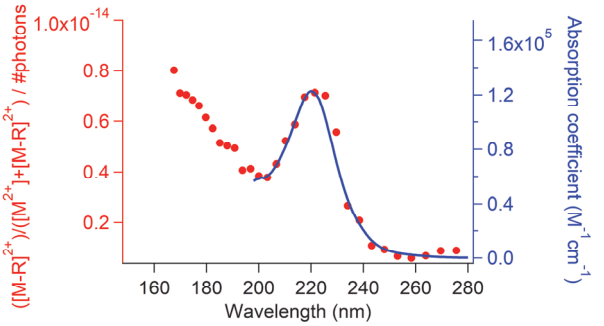

Fig. 4. Comparison between absorption spectrum of TinOH in EtOH solution (blue line) and yield of $[M\text{-}R]^{2+}$ in the gas phase (red dots). This ion yield spectrum was calculated from the ratio of the fragment peak to the total of the main peak plus the fragment peak, divided by the photon flux at different energies.

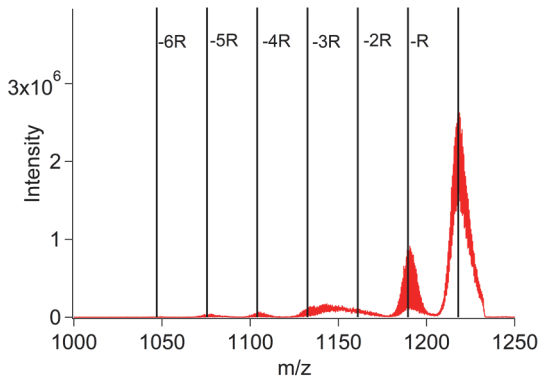

Fig. 5. Mass spectrum with incident light of 92 nm (13.5 eV). Vertical lines indicate the main peak (*m/z* = 1218) and peaks indicating various butyl chain losses.

shows a clear increase in absorption below 200 nm.

At VUV energies, between 7 and 13.5 eV, the fragmentation yield increased gradually with photon energy. Additionally, different fragments could be observed. This is shown in Fig. 5. As can be seen, fragmentation is much stronger at these higher energies (compare the signal intensities in Figs. 3 and 5, which are corrected for the photon fluxes). The M-R fragment is again the strongest, although multiple butyl chain loss (up to M-6R) is now detected as well. The subsequent fragmentation reactions are likely to be a result of the higher internal energy that remains in the various $(M\text{-}nR)^{2+}$ intermediates at higher photon energies.

Photons with energy >12 eV could ionize the tin cage, promoting it from a 2+ to a 3+ charge. The intact tin cage with a 3+ charge could not be detected, but a 3+ cage having lost one butyl chain could (see Fig. 6).

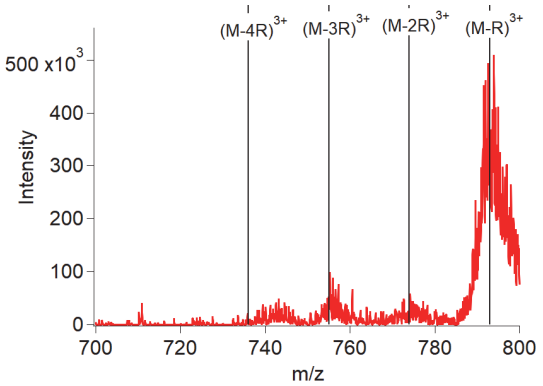

Fig. 6. Mass spectrum with incident light at 13.5 eV (92 nm), in the 3+ range of the spectrum. Vertical lines indicate the peaks corresponding to loss of multiple butyl groups.

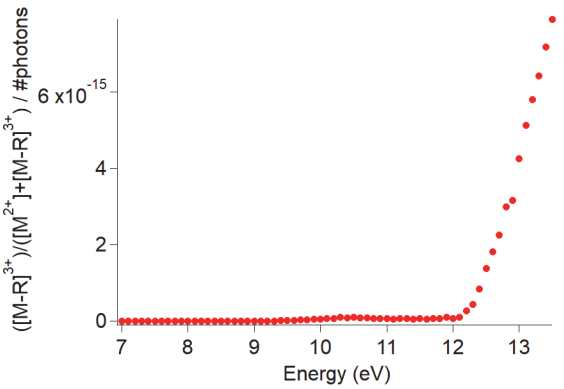

Fig. 7. Fragmentation yield of $(M\text{-}R)^{3+}$. This fragmentation yield was obtained by dividing the area of the fragment peak by that of the main peak plus the fragment peak, and dividing by the photon flux.

It is likely that upon photoionization of the cage, the resulting radical trication is unstable and cleaves off one butyl group. The isotope pattern of the peaks unequivocally indicates a 3+ charge. 3+ fragments only appear with a photon energy above the ionization threshold, clearly visible in Fig. 7 around 12.1 eV.

4. Conclusion

Tin-oxo cages were exposed to UV and VUV light (4-13.5 eV) and the fragmentation pathways were studied. Butyl chain loss was the main photoreaction channel, occurring above the electronic absorption threshold of about 5 eV (~250 nm). The higher the photon energy, the higher the fragmentation yield (defined as the integral of the fragments divided by the main peak, corrected for the photon flux). Above the ionization threshold of ~12.1 eV, the charge of the tin cage could be promoted from 2+ to 3+ and one or more butyl chains are lost.

Although the energies used in this work are much lower than those used in EUV lithography, these lower energy experiments are relevant to EUV lithography for two reasons. Firstly, EUV photons (92 eV) induce a cascade of secondary electrons, which have lower energies and may cause excitations much like the photons used here. Secondly, EUV sources often contain VUV out-of-band radiation, which implies that the effect of VUV on photoresist materials should be considered. Most importantly, this study gives fundamental insight into the properties of the tin-oxo cages and emphasizes the facile breaking of the tin-carbon bonds as a key reaction.

Acknowledgements

Part of this work has been carried out at the Advanced Research Center for Nanolithography (ARCNL), a public-private partnership of the University of Amsterdam (UvA), the VU University Amsterdam (VU), the Netherlands Organisation for Scientific Research (NWO) and the semiconductor equipment manufacturer ASML. The authors acknowledge Ed Zuidinga (UvA) for initial testing of the electrospray conditions and thank Niklas Ottosson, Thomas Schlathölter and Ronnie Hoekstra for performing preliminary experiments that initiated this research. We warmly thank the whole SOLEIL staff for running the facility under project 20161099.

References

1. J. Passarelli, M. Murphy, R. del Re, M. Sortland, L. Dousharm, M. Vockenhuber, Y. Ekinci, M. Neisser, D. A. Freedman, and R. L. Brainard, *Proc. SPIE*, **9425** (2015) 94250T.
2. H. Nakagawa, T. Naruoka, and T. Nagai, *J. Photopolym. Sci. Technol.*, **27** (2014) 739.
3. R. P. Oleksak, R. E. Ruther, F. Luo, K. C. Fairley, S. R. Decker, W. F. Stickle, D. W. Johnson, E. L. Garfunkel, G. S. Herman, and D. A. Keszler, *ACS Appl. Mater. Interfaces*, **6** (2014) 2917.
4. R. Fallica, J. K. Stowers, A. Grenville, A. Frommhold, A. P. G. Robinson, and Y. Ekinci, *J. Micro/Nanolith. MEMS MOEMS*, **15** (2016) 33506.
5. K. D. Closser, D. F. Ogletree, P. Naulleau, and D. Prendergast, *J. Chem. Phys.*, **146** (2017) 164106.
6. S. Bhattarai, W. Chao, S. Aloni, A. R. Neureuther, and P. P. Naulleau, *Proc. SPIE*, **9422** (2015) 942209.
7. P. Naulleau, C. Anderson, W. Chao, S. Bhattarai, and A. Neureuther, *J. Photopolym. Sci. Technol.*, **27** (2014) 747.
8. M. Carcasi, D. Bassett, W. Printz, S. Kawakami, and Y. Miyata, *Proc. SPIE*, **8325** (2012) 83250K.

9. B. Cardineau, R. del Re, M. Marnell, H. Al-Mashat, M. Vockenhuber, Y. Ekinci, C. Sarma, D. A. Freedman, and R. L. Brainard, *Microelectron. Eng.*, **127** (2014) 44.
10. C. Eychenne-Baron, F. Ribot, and C. Sanchez, *J. Organomet. Chem.*, **567** (1998) 137.
11. J. Haitjema, Y. Zhang, M. Vockenhuber, D. Kazazis, Y. Ekinci, and A. M. Brouwer, *J. Micro/Nanolith. MEMS MOEMS*, **16** (2017) 033510.
12. R. Fallica, J. Haitjema, L. Wu, S. Castellanos, F. Brouwer, and Y. Ekinci, *Proc. SPIE*, **10143** (2017) 101430A.
13. S. Saha, D.-H. Park, D. C. Hutchinson, M. R. Olsen, L. N. Zakharov, D. Marsh, S. Goberna-Ferrón, R. T. Frederick, J. T. Dulius, N. Kenane, G. S. Herman, D. W. Johnson, D. A. Keszler, and M. Nyman, *Angew. Chem. Int. Ed.*, **56** (2017) 10140.
14. D. Egorov, L. Schwob, M. Lalande, R. Hoekstra, and T. Schlathölter, *Phys. Chem. Chem. Phys.*, **18** (2016) 26213.
15. A. Giuliani, A. R. Milosavljević, F. Canon, and L. Nahon, *Mass Spectrom. Rev.,* **33** (2014) 424.
16. S. Daly, M. Krstic, A. Giuliani, R. Antoine, L. Nahon, A. Zavras, G. N. Khairallah, V. Bonacic-Koutecky, P. Dugourd, and R. A. O'Hair, *Phys. Chem. Chem. Phys.,* **17** (2015) 25772.
17. J. Zhen, S. R. Castillo, C. Joblin, G. Mulas, H. Sabbah, A. Giuliani, L. Nahon, S. Martin, J.-P. Champeaux, and P. M. Mayer, *Astrophys. J.*, **822** (2016) 113.
18. D. Dakternieks, H. Zhu, E. R. T. Tiekink, and R. Colton, *J. Organomet. Chem.*, **476** (1994), 33.
19. L. Van Lokeren, R. Willem, D. van der Beek, P. Davidson, G. A. Morris, and F. Ribot, *J. Phys. Chem. C.*, **14** (2010) 16087.
20. A. R. Milosavljević, C. Nicolas, J. F. Gil, F. Canon, M. Réfrégiers, L. Nahon, and A. Giuliani, *J. Synchrotron Rad.*, **19** (2010) 174.
21. L. Nahon, N. de Oliviera, G. Garcia, J. F. Gil, B. Pilette, O. Marcouille, B. Lagarde, and F. Polack, *J. Synchrotron Rad.,* **19** (2012) 508.
22. J. Haitjema, Y. Zhang, N. Ottosson, and A. M. Brouwer, *J. Photopolym. Sci. Technol.*, **30** (2017) 99.